Optics Letters

Solid-state FMCW LiDAR with in-fiber beam scanner

Zhi Li,[1,†] Bonan Liu,[2,3,†] Chang Rui Liao,[2,3] and H. Y. Fu[1,*]

[1]Tsinghua Shenzhen International Graduate School and Tsinghua–Berkeley Shenzhen Institute (TBSI), Tsinghua University, Shenzhen 518055, China
[2]Key Laboratory of Optoelectronic Devices and Systems of Ministry of Education, College of Physics and Optoelectronic Engineering, Shenzhen University, Shenzhen 518060, China
[3]Shenzhen Key Laboratory of Photonic Devices and Sensing Systems for Internet of Things, Guangdong and Hong Kong Joint Research Centre for Optical Fibre Sensors, Shenzhen University, Shenzhen 518060, China
*Corresponding author: hyfu@sz.tsinghua.edu.cn
†These authors contributed equally to this Letter.

Received 19 August 2021; revised 8 November 2021; accepted 23 November 2021; posted 29 November 2021; published 16 January 2022

The beam scanner is a predominant part in the light detection and ranging (LiDAR) system to achieve three-dimensional (3D) imaging. The solid-state beam-steering device has emerged as a promising candidate technology for a beam scanner with the advantages of robustness, stability, and high scanning speed. Here we propose a frequency modulated continuous wave (FMCW) LiDAR system with an in-fiber solid-state beam scanner. A 45° tilted fiber grating (TFG) is first employed to achieve in-fiber solid-state spectral scanning in the LiDAR system. A maximum output efficiency of 93.7% is achieved with proper polarization control. A single-mode fiber is then used to fabricate a 2-cm 45° TFG, which significantly reduces the size and the cost of the beam scanner in the LiDAR system. We experimentally realize 3D imaging of targets placed at a distance of 1.2 m based on our proposed LiDAR system. In addition, the system can achieve a detection distance of 6 m with a ranging precision of 24 mm.

https://doi.org/10.1364/OL.440940

A light detection and ranging (LiDAR) system as a three-dimensional (3D) sensor can achieve long-distance and high-accuracy 3D imaging [1]. The LiDAR system has been extensively applied in many industrial and scientific areas, such as virtual reality (VR) and augmented reality (AR) video games, mapping, remote sensing, and autonomous driving systems. [2–5]. The beam scanner plays the most crucial role in a LiDAR system, which is used to steer a beam in different directions to acquire a 3D map of the surrounding environment. Traditional LiDAR systems are based on mechanical beam-steering devices such as galvanometers that are bulky, expensive, prone to failure, and slow. Consequently, solid-state LiDARs with no moving parts are desirable to achieve stable and fast beam scanning. Many solid-state beam-scanning technologies have been developed and have attracted much attention, such as optical phased array (OPA) and the mirror of microelectromechanical systems (MEMS) [6–8]. The MEMS mirror greatly minimizes the size of the beam scanner to several centimeters with an improved scanning speed of several kilohertz. The OPA further improves the beam-steering speed by accurately controlling the optical phase, which can achieve a maximum scanning speed on the megahertz scale. Recently, a spectral-scanning method was proposed to realize an ultrafast 3D imaging LiDAR system by combining a wavelength-swept laser source with diffractive optics [9]. Such an ultrafast spectral-scanning technique has been used in various types of LiDAR systems including pulse LiDAR systems, frequency-modulated continuous-wave (FMCW) LiDAR systems, and amplitude-modulated continuous-wave (AMCW) LiDAR systems [10–13]. Previously, our group proposed a LiDAR by cascading a virtually imaging phased array (VIPA) and a diffractive grating to realize two-dimensional (2D) ultrafast beam-steering [14,15]. A diffractive grating is the most widely employed diffractive optical component in the LiDAR system. However, a free space diffractive grating has relatively high cost, limited diffraction efficiency, and is bulky. These drawbacks will further hinder the development of spectral-scanning LiDAR.

In this work, we demonstrate an implementation of an in-fiber grating as the beam-steering device for FMCW LiDAR. The beam steering is achieved by using a wavelength-swept laser source. The in-fiber beam scanner is made by a 45° tilted fiber grating (TFG). Our home-made 45° TFG can achieve a maximum diffractive efficiency of 93.7%, which can further improve the output power of the LiDAR system if compared with a free-space grating. The fiber-based steering component is much more flexible and compact. Thus, our proposed in-fiber beam scanner also has the advantages of easy installation, small size, and low cost. The 45° TFG has already been applied as a beam scanner in infrared optical wireless communication (OWC) systems [16,17]. Furthermore, benefiting from its high diffractive efficiency and small size, the 45° TFG has widespread applications, such as in intensity imaging, widely wavelength-tunable mode-locked fiber lasers, and free-space fiber couplers [18–20]. To the best of our knowledge, this is the first time that 45° TFG is proposed to be used in a LiDAR system. We experimentally prove its feasibility in 3D imaging and long-range detection.

The principle of beam steering based on a 2-cm 45° TFG is demonstrated in Fig. 1. The incident light will propagate through the active region of the 45° TFG with the core mode. Then the forward propagating light will be transformed into radiation

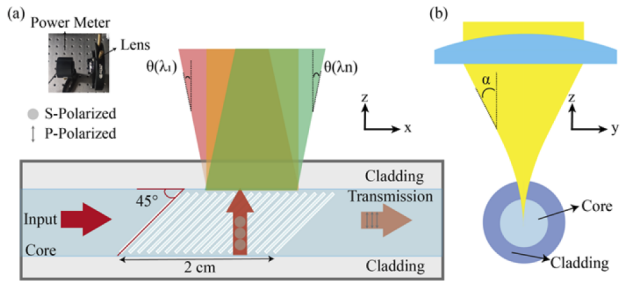

Fig. 1. Sketch of a 45° TFG displaying the emission geometry. (a) Principle of TFG-based beam-steering method. (b) Divergent angle of output beam along the *y*-axis direction.

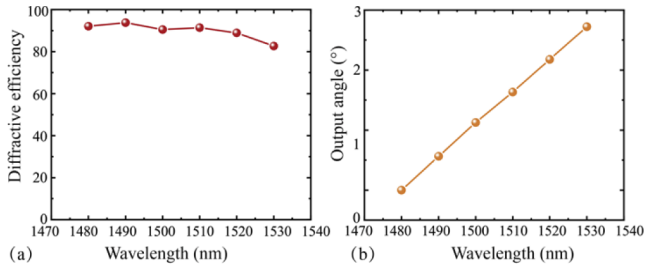

Fig. 2. (a) Diffraction efficiency of 45° TFG with different wavelengths. (b) Output angle from 45° TFG with different wavelengths.

modes, which is a unique feature of 45° TFG. The diffractive light will directly output into free space. However, only s-polarized light in the fiber core can be radiated out. Meanwhile, the p-polarized light continues to propagate along the fiber core. The polarization-dependent loss can reach approximately 40 dB [21]. The 45° TFG works as an in-fiber grating to achieve spectral scanning for the LiDAR system.

As shown in Fig. 1(a), light beams with different wavelengths will output in different directions. The 45° TFG is also a wavelength-independent diffractive optical component. Theoretical analysis of the radiation mode has been reported based on the phase-matching condition [22]. The diffractive angle of radiation mode from core mode to cladding mode can be given by

$$\cot(\theta_{out}) = \cot(\theta_t) - \frac{n\Lambda}{\lambda \sin\theta_t}, \tag{1}$$

where θ_{out} is the diffractive angle of the radiation mode, θ_t is the tilted angle of the TFG, Λ is the grating period, and n is the refractive index of the fiber core. Considering the refraction that occurs at the interface between the cladding mode and air, the final diffractive angle of the radiation mode can be expressed as

$$\sin(\theta_{out}) = \frac{n \cdot (\cot\theta_t - \frac{n\Lambda}{\lambda \sin(\theta_t)})}{\sqrt{1 + (\cot\theta_t - \frac{n\Lambda}{\lambda \sin(\theta_t)})}}. \tag{2}$$

Based on the relationship between Λ and θ_{out} of the TFG,

$$\Lambda \cos(\theta_t) = \frac{\lambda}{2n}, \tag{3}$$

eventually, the angular dispersion equation can be described as [22]

$$\frac{\partial\theta_{out}}{\partial\lambda} = -\frac{\sin(2\theta_t)}{\lambda}. \tag{4}$$

From Eq. (4), we can conclude that the angular dispersion of the TFG is maximum when the tilted angle θ_t is 45°. Thus, the angular dispersion at 1500 nm is approximately 0.038°/nm. The beam intensity distribution pattern after output from the 45° TFG has been analyzed in detail in an earlier work [23]. There is an exponential decay of the optical power along the length of the 45° TFG. Owing to the refraction in the *y*-axis direction, a light beam with divergent angle α will output from the fiber, as shown in Fig. 1(b). Here, α can be calculated by

$$\alpha = \arcsin(NA), \tag{5}$$

where NA is the numerical aperture of the fiber [24].

The used 45° TFG was fabricated using femtosecond laser direct inscription [25]. The laser pulses were generated at 515 nm with a repetition rate of 200 kHz and a duration of 290 fs. Through an oil-immersed 100× objective lens, the pulses were focused onto a single-mode optical fiber (YOFC). An air-bearing translation stage (Aerotech) was implemented to mount the single-mode fiber and to ensure accurate motion control. The grating was induced in a line-by-line manner with the segments crossing the fiber core. The grating obtained possessed a grating pitch of 1 μm, a tilt angle of 45°, and a grating length of 20 mm.

We experimentally measured the dispersive angles over a bandwidth of 50 nm (from 1480 to 1530 nm) and its corresponding diffractive efficiency based on our homemade 45° TFG, as shown in Fig. 2. To measure the output power of the beam into the free space, a short focal length lens and a free-space power meter (S148C, Thorlabs) were used, as shown in the inset picture in Fig. 1(a). Because the light of the radiation mode from the 45° TFG is polarization independent, a polarization controller is used to change the polarization state of the incident light. By adequate adjustment, the maximum diffractive efficiency reached 93.7%, as shown in Fig. 2(a). By changing the wavelength of the incident light with a bandwidth of 50 nm, the beam-steering field of view (FoV) was 2.7°. However, the output angle changed accordingly along with the wavelength change, as shown in Fig. 2(b). The above measurements exhibited a good beam-steering performance of the 45° TFG as a diffractive optical element.

Figure 3(a) shows a schematic diagram of the experimental set-up for FMCW LiDAR system with an in-fiber beam scanner. We adopted a coaxial LiDAR system structure which is simple and compact. Consequently, the collection capability of echo signals from the target was relatively weak for the small receive aperture of the 45° TFG [26]. Thus, a coherent detection method was introduced in our system to greatly reduce the interference from environmental light and detect weak echo signals. A wavelength-swept laser (TSL710, Santec) with a linewidth of 100 kHz was used as the laser source, which can offer a coherent length of over 100 meters for FMCW ranging. The incident light from the laser source was launched into two arms after propagating through a power splitter. Both arms were Mach–Zehnder interferometers [27]. The power was split with 99% going into the measurement arm and the residual 1% fed into an auxiliary arm, which was used to suppress the effects of nonlinear frequency sweeps in the data processing [28]. In the measurement arm, 10% of the power of light went into a local arm, which was used as the local signal and compensated for the extra introduced fiber length by the polarization controller (PC) and 45° TFG. A trigger signal from the tunable laser was applied to help sample the data for each frequency sweep [15].

The beam-steering part with a 2-cm active length of the TFG is shown in Fig. 3(b). Thus, a cylindrical lens with a size of 20 mm

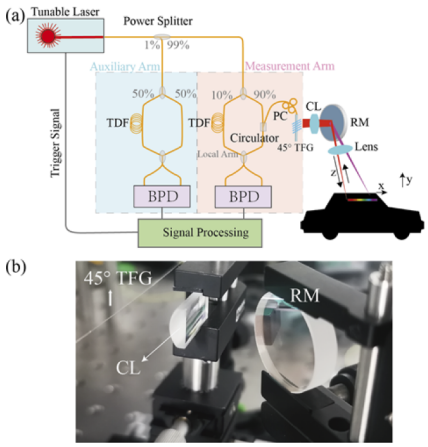

Fig. 3. (a) Schematic diagram of 45° TFG-based FMCW LiDAR system. (b) Picture of the beam-steering part. TDF, time delay fiber; PC, polarization controller; CL, cylindrical lens; BPD, balanced photodetection; RM, reflective mirror.

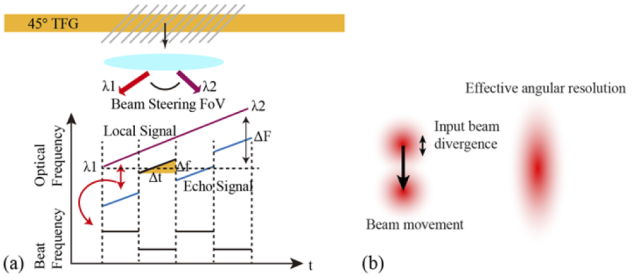

Fig. 4. (a) Working principle of TFG-based spectral-scanning FMCW LiDAR. (b) Stretching of angular resolution caused by dispersion-scanning coherent ranging.

× 10 mm was used to collimate the beam from the 45° TFG. A reflective mirror was adopted to adjust the output direction of the light beam. A plano-convex lens was used to minimize the beam size. The ranging principle of such a swept-source FMCW LiDAR is shown in Fig. 4(a). We assume that the frequency of the swept laser source is linearly changed with time. The purple line is the frequency in the local arm. During the process of a wavelength sweep, the output direction of the laser beam is varied by the 45° TFG at the same time. The blue line demonstrates the echo signal with a time delay caused by the round-trip time, which is reflected from the scanned target. The echo signal and local signal will be mixed with each other at a balanced photodetector (BPD). The beat signal is thus generated, as shown by the gray line. The frequency of the beat signal can be used to calculate the round-trip time. Thus, such a spectral scanning FMCW LiDAR system can achieve beam steering and distance detection at the same time. The division of the time window and calculation of the beat frequency for a ranging point is conducted by using a short-time Fourier transform (STFT) in the post data processing. However, a sub-bandwidth Δf will be scanned over for a point in the FMCW ranging. Thus, the effective angular resolution is stretched along the dispersion-scanning trace, as demonstrated in Fig. 4(b). With the increment of Δf, the ranging resolution will be improved. However, the angular resolution will be worse. Thus, there is a trade-off between angular resolution and ranging resolution.

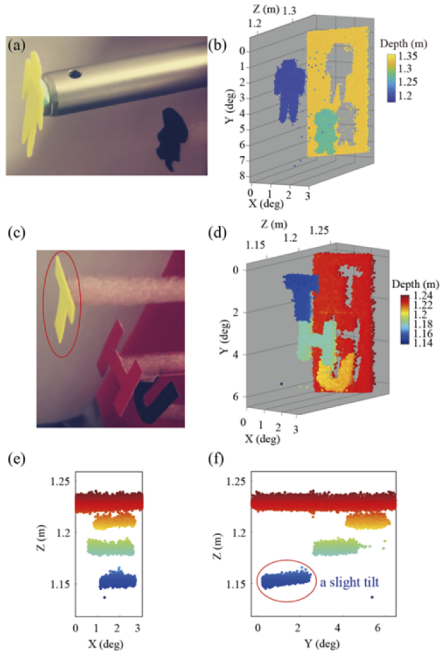

Fig. 5. 3D imaging results. The vertical scan is performed by a rotatable mirror. (a) Picture of the targets (two pieces of cardboard) placed at approximately 1.2–1.3 m distance. (b) Depth map of two pieces of cardboard cut into human shapes. (c) Picture of the targets (three pieces of cardboard) with a closer interval distance. (d) Depth map of the two targets with Tsinghua University logo. (e), (f) Projections of the 3D image along the *y*-axis and *x*-axis.

To demonstrate the feasibility of the in-fiber grating in the LiDAR system, an experiment to obtain 3D cloud points of targets was conducted. The 3D imaging results are provided in Fig. 5. The targets were placed at a distance of approximately 1.2 m and the laser wavelength was changed from 1480 to 1530 nm in 0.5 seconds. The spectral scanning direction was along the *x*-axis with a scanning FoV of 2.7°. The total frequency tuning range ΔF was approximately 6.6 THz. The generated beat signals at the BPD was sampled by an oscilloscope (MSO73304DX, Tektronix). Then a short-time Fourier transform was used to acquire the frequency spectrum at different ranging points. Here, the bandwidth used for a point ranging Δf was approximately 41 GHz. The corresponding time window length Δt was approximately 3 ms. For FMCW ranging, the theoretical ranging precision can be calculated by $c/2\Delta f$, where c is the speed of light. A better ranging precision can be obtained with the larger bandwidth Δf. It should be noted that the time-window length Δt for each point ranging is adjustable with the data processing. In other words, the bandwidth Δf for FMCW ranging is reconfigurable, which can further adjust the ranging precision and imaging pixels $\Delta F/\Delta f$. At first, two pieces of cardboard that were cut to resemble a human shape were placed at different distances, as shown in Fig. 5(a). The distance interval between the two figures was approximately 6 cm. The 3D imaging results are shown in Fig. 5(b). The outline of the targets was clearly observed. The spectral-scanning technique used showed good performance for the lateral resolution and ranging resolution. Additionally, we also measured the targets with a closer distance between each other. As presented in Fig. 5(c), three cardboards in the shape of "THU" letters were placed with 1–3 centimeters distance between each letter. The 3D imaging result

is given in Fig. 5(d). Figures 5(e) and 5(f) are the projections of the 3D imaging along the y-axis and x-axis, respectively. We note that a slight tilt on the surface of the letter "T" can be clearly observed, as exhibited by the red circles in Figs. 5(c) and 5(f). The results demonstrate a good ranging resolution of our proposed LiDAR system. To demonstrate the performance of the long-range detection, a target was placed 6 meters away from the beam-steering part. The wavelength swept range for the measurement was from 1480 to 1480.1 nm. We measured the ranging precision with different bandwidths Δf.The ranging precision was obtained by calculating the standard deviation of the measured results over 20 times. As shown in Fig. 6(a), the ranging precision can be 2.4 mm with a bandwidth of 30 GHz for a ranging point. When the bandwidth Δf allocated for a point ranging is decreased gradually, the ranging precision becomes worse. When the bandwidth is changed to 2 GHz, a cm-level ranging resolution is achieved. Figure 6(b) shows the STFT signals for targets at 6 m with different bandwidths (time window length). The signal-to-noise ratio (SNR) is gradually reduced along with the decrease of Δf, which agrees well with the results in Fig. 6(a).

In conclusion, we propose a FMCW LiDAR system with an in-fiber beam scanner. A homemade 45° tilted fiber grating is employed as a diffractive optical element to achieve a spectral scanning function of the LiDAR system. The in-fiber grating greatly compensates for the drawbacks of free space diffractive grating used in traditional spectral scanning LiDAR systems, such as being bulky, expensive, difficult to install, and having low diffractive efficiency. A single fiber after being fabricated using femtosecond laser direct inscription can be implemented in a LiDAR system. The in-fiber spectral scanner caters to the needs of the LiDAR system in beam scanners, which are small size, low cost, and robust. With the rapid development of the fiber-to-the-home, our technique thus holds promise for miniaturized 3D sensors, which are able to be deployed for indoor applications.

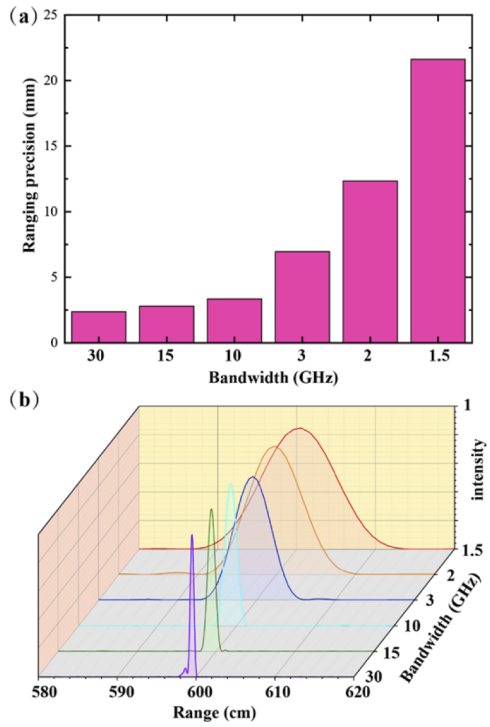

Fig. 6. Ranging results with target placed at a distance of 6 m. (a) Ranging precision with different bandwidths Δf for the points of the FMCW ranging. (b) FFT signal for ranging points with different bandwidths Δf.

Funding. Science, Technology and Innovation Commission of Shenzhen Municipality (WDZC20200820160650001); Shenzhen Technology and Innovation Council (JCYJ20180507183815699); Overseas Research Cooperation Fund of Tsinghua Shenzhen International Graduate School (HW2020006); Basic and Applied Basic Research Foundation of Guangdong Province (2021A1515011450).

Disclosures. The authors declare no conflicts of interest.

Data availability. Data underlying the results presented in this paper are not publicly available at this time but may be obtained from the authors upon reasonable request.

REFERENCES

1. B. Schwarz, Nat. Photonics **4**, 429 (2010).
2. D. Droeschel and S. Behnke, in *2018 IEEE International Conference on Robotics and Automation (ICRA)* (IEEE, 2018), 5000–5007.
3. H. Wang, B. Wang, B. Liu, X. Meng, and G. Yang, Rob. Auton. Syst. **88**, 71 (2017).
4. J. McCormack, J. Prine, B. Trowbridge, A. C. Rodriguez, and R. Integlia, in *2015 IEEE Games Entertainment Media Conference (GEM)* (IEEE, 2015), 1–5.
5. M. A. Lefsky, W. B. Cohen, G. G. Parker, and D. J. Harding, BioScience **52**, 19 (2002).
6. S. T. Holmström, U. Baran, and H. Urey, J. Microelectromech. Syst. **23**, 259 (2014).
7. J. Sun, E. Timurdogan, A. Yaacobi, E. S. Hosseini, and M. R. Watts, Nature **493**, 195 (2013).
8. Y. Wang, G. Zhou, X. Zhang, K. Kwon, P.-A. Blanche, N. Triesault, K.-S. Yu, and M. C. Wu, Optica **6**, 557 (2019).
9. N. Li, C. P. Ho, I.-T. Wang, P. Pitchappa, Y. H. Fu, Y. Zhu, and L. Y. T. Lee, Nanophotonics **10**, 1437 (2021).
10. Y. Jiang, S. Karpf, and B. Jalali, Nat. Photonics **14**, 14 (2020).
11. M. Okano and C. Chong, Opt. Express **28**, 23898 (2020).
12. J. Riemensberger, A. Lukashchuk, M. Karpov, W. Weng, E. Lucas, J. Liu, and T. J. Kippenberg, Nature **581**, 164 (2020).
13. Z. Zhang, C. Zhang, T. Shirahata, S. Yamashita, and S. Y. Set, in *CLEO: Applications and Technology* (Optical Society of America, 2020), paper JTu2G.34.
14. Z. Li, Z. Zang, H. Y. Fu, Y. Luo, and Y. Han, Appl. Opt. **60**, 2177 (2021).
15. Z. Li, Z. Zang, Y. Han, L. Wu, and H. Fu, Opt. Express **29**, 16547 (2021).
16. G. Wang, U. Habib, Z. Yan, N. J. Gomes, Q. Sui, J.-B. Wang, L. Zhang, and C. Wang, J. Lightwave Technol. **36**, 4618 (2018).
17. G. Wang, L.-Y. Shao, D. Xiao, S. Bandyopadhyay, J. Jiang, S. Liu, W. Li, C. Wang, and Z. Yan, J. Lightwave Technol. **39**, 83 (2021).
18. B. Lu, C. Zou, Q. Huang, Z. Yan, Z. Xing, M. Al Araimi, A. Rozhin, K. Zhou, L. Zhang, and C. Mou, J. Lightwave Technol. **37**, 3571 (2019).
19. G. Wang, C. Wang, Z. Yan, and L. Zhang, Opt. Lett. **41**, 2398 (2016).
20. S. Bandyopadhyay, L.-Y. Shao, W. Chao, Z. Yan, F. Hong, G. Wang, J. Jiang, P. Shum, X. Hong, and W. Wang, Opt. Express **28**, 16569 (2020).
21. K. Zhou, G. Simpson, X. Chen, L. Zhang, and I. Bennion, Opt. Lett. **30**, 1285 (2005).
22. H. Qin, Z. Yan, Q. Sun, G. Wang, C. Wang, D. Liu, and L. Zhang, in *2017 Opto-Electronics and Communications Conference (OECC) and Photonics Global Conference (PGC)* (IEEE, 2017), 1–3.
23. H. Qin, Q. He, Z. Xing, X. Guo, Z. Yan, Q. Sun, K. Zhou, H. Wang, D. Liu, and L. Zhang, J. Lightwave Technol. **37**, 1 (2019).
24. S. Remund, A. Bossen, X. Chen, L. Wang, A. Adebayo, L. Zhang, B. Považay, and C. Meier, *SPIE BiOS* (SPIE, 2014), Vol. 8938, paper 89381E.
25. K. Yang, C. Liao, S. Liu, J. He, J. Wang, and Y. Wang, J. Lightwave Technol. **38**, 1474 (2020).
26. J. H. Leach, S. R. Chinn, and L. Goldberg, Appl. Opt. **54**, 9752 (2015).
27. B. Behroozpour, P. A. Sandborn, M. C. Wu, and B. E. Boser, IEEE Commun. Mag. **55**, 135 (2017).
28. F. Ito, X. Fan, and Y. Koshikiya, J. Lightwave Technol. **30**, 1015 (2012).